AGU PUBLICATIONS

Geophysical Research Letters

RESEARCH LETTER

10.1002/2015GL063298

Key Points:
- Spontaneous adjustment mechanism gives required GW forcing for climate models
- Source-related GW annual cycle and realistic EP flux intermittency are produced

Correspondence to:
A. de la Cámara,
acamarai@lmd.ens.fr

Citation:
de la Cámara, A., and F. Lott (2015), A parameterization of gravity waves emitted by fronts and jets, *Geophys. Res. Lett.*, *42*, 2071–2078, doi:10.1002/2015GL063298.

Received 28 JAN 2015
Accepted 25 FEB 2015
Accepted article online 27 FEB 2015
Published online 31 MAR 2015

A parameterization of gravity waves emitted by fronts and jets

A. de la Cámara[1] and F. Lott[1]

[1] Laboratoire de Météorologie Dynamique, IPSL, CNRS, École Normale Supérieure, Paris, France

Abstract Based on the theoretical and experimental facts that gravity waves (GWs) can be spontaneously emitted during the evolution of a near-balanced flow, a stochastic parameterization of GWs linked to fronts and jets is proposed. Although the spontaneous adjustment theory used predicts "exponentially" small GW fields, it is shown that it is sufficient to produce realistic GW drag at mesospheric levels. Off-line tests using reanalyzed meteorological fields are conducted and show that the GWs emitted present a strong annual cycle following that of the sources. Also, the GW momentum fluxes in the lower stratosphere are qualitatively realistic in terms of intermittency. Online tests in a middle atmosphere general circulation model show that the scheme can potentially perform as well as highly tuned existing GW schemes.

1. Introduction

Internal gravity waves (GWs) propagating vertically from their tropospheric sources force the circulation of the middle atmosphere; i.e., they are crucial for the closure of the jets at mesospheric levels and for the maintenance of the quasi-biennial oscillation (QBO) [*Holton*, 1983]. Their spatial scales being too small to be represented in Earth system models (ESMs) at present, they need to be parameterized. While the parameterization of GWs due to orography is relatively well understood [*Lott*, 1999]; the GWs emitted by convection, fronts, and jets are often represented using uniform sources [*Warner and McIntyre*, 1996; *Hines*, 1997]. Although this is somehow justified by the fact that GWs are strongly filtered by the background flow, there remains the issue that the waves sources present no annual cycle and do not vary when the climate changes. For these reasons, parameterizations of convective sources have been developed over the last decade [*Beres et al.*, 2004; *Song and Chun*, 2005] and made sufficiently efficient to help models internally generate a QBO [*Lott and Guez*, 2013; *Schirber et al.*, 2014].

Parameterizations of GWs issued from fronts and jets are less frequently used, with the exceptions of *Charron and Manzini* [2002] and *Richter et al.* [2010] who used a frontogenesis function to detect the locations from where the GWs are launched. Nevertheless, at the time those works were published the partition of the response to an ageostrophic frontogenesis forcing between the balanced response and the GWs was still an unsolved theoretical problem, so these authors made the reasonable decision of emitting a fixed amount of GW momentum flux wherever the frontogenesis function exceeded a certain threshold: there is no link between the magnitude of the frontogenesis function itself and the GW amplitude.

There have been recent developments in the generation of gravity waves in the vicinity of jets and fronts on both theoretical and experimental sides [e.g., *Williams et al.*, 2005; *Borchert et al.*, 2014], and today the mechanisms of spontaneous adjustment where a near-balanced flow emits GWs during its evolution are much better understood (see the review by *Plougonven and Zhang* [2014, and references therein]). Among the available theories, *Lott et al.* [2010] and *Lott et al.* [2012b] investigate the linear emission of GWs by potential vorticity (PV) anomalies in a vertically sheared wind and show that a PV anomaly produces a GW Eliassen-Palm (EP) flux given by the following:

$$\mathcal{F} = \frac{F_0}{4} e^{-\pi\sqrt{J}}, \text{ where } F_0 = \frac{\rho_r g^2}{f\theta_r^2 N^3} \left(\rho_r q_r \sigma_z\right)^2 . \tag{1}$$

Here g is the gravity constant, f the Coriolis parameter, N is the buoyancy frequency, $J = N^2/\Lambda^2$ is the Richardson number (Λ is the vertical shear of the horizontal wind), ρ_r and θ_r are reference density and potential temperature, q_r is the amplitude of the PV anomaly, and σ_z is its depth.

In equation (1) the exponentially small term translates the fact that immediately above the PV anomaly the dynamics is almost quasi-geostrophic and the disturbance produced by the PV decays exponentially with

altitude. This decay ceases at the inertial level above the PV anomaly, where the intrinsic frequency equals the Coriolis frequency: the disturbance becomes an upward propagating GW. Note that the exponential smallness predicted by the theory is in disagreement with some experimental observations [*Williams et al.*, 2008], although the mechanisms of GW generation in these experiments are not clear yet [*Plougonven and Zhang*, 2014]. Using equation (1) is adapted to represent GWs emitted by fronts, since within fronts relative vorticity anomalies and vertical wind shear are large. Interestingly, using (1) can also recover the approach using frontogenesis forcing (at least in part), since this forcing produces relative vorticity anomalies. In this case, our GWs can be viewed as a late consequence of the frontogenesis forcing.

In the present paper, we apply the stochastic methods described by *Eckermann* [2011], *Lott et al.* [2012a], and *Lott and Guez* [2013] to construct a GW parameterization directly linked to frontal sources (hereafter referred to as FGWD), adapting almost literally equation (1). The plan of the paper is as follows: Section 2 describes the formalism used and recalls some of the reasons that justify a stochastic approach. Section 3 analyzes some characteristics of the GWs generated in off-line setup, such as intermittency and annual cycle of the momentum fluxes, and section 4 tests the parameterization online in the Laboratoire de Météorologie Dynamique zoom (LMDz) general circulation model (GCM). Finally, section 5 discusses the impact of our results on the improvement of the representation of the annual cycle in ESMs, as well as on future climate projections.

2. Formalism

The formalism used in the present study adapts the stochastic approach used by *Lott and Guez* [2013] to parameterize convectively generated GWs. Basically, it consists on working with a stochastic series of few monochromatic waves whose wave properties are chosen randomly. The justification for this approach is twofold. On the one hand, the use of few monochromatic waves mimics the observations of rather narrow-banded GW packets in the lower stratosphere [*Hertzog et al.*, 2008]. On the other hand, the stochastic sampling of the GW field and the random choice of wave properties deals with the inherent unpredictability of subgrid-scale dynamics from the large-scale conditions [*Palmer et al.*, 2005] and also mimics the intermittent nature of the GW field [*Hertzog et al.*, 2012]. In addition, the present approach produces fairly realistic GW energy spectrum as a function of the vertical wave number [*de la Cámara et al.*, 2014].

To adapt the method to frontal waves, we first represent the subgrid-scale potential vorticity anomaly as a stochastic "Fourier" series:

$$q' = \sum_{n=1}^{\infty} C_n \hat{q}_n e^{i\left(\vec{k}_n \cdot \vec{x} - \omega_n t\right)}, \tag{2}$$

where $\hat{q}_n$ is the amplitude of the nth harmonic of the subgrid-scale PV anomaly q', $\vec{k}_n$ and ω_n its horizontal wave number and ground-based frequency, and C_n^2 is the probability of the nth wave to represent the entire wave field. We choose randomly $\vec{k}_n$ and ω_n but directly relate the amplitude $\hat{q}_n$ to the large-scale relative vorticity field $\zeta_r : \rho_r \hat{q}_n \approx \zeta_r \bar{\theta}_{0,z}$. Three approximations have been done here. The first consists in relating the grid-scale PV anomaly to the grid-scale relative vorticity anomaly (neglecting for instance the term involving the vertical derivative of the temperature anomaly), which we think is both quantitatively and qualitatively reasonable. The second is to consider that the subgrid-scale standard deviation is equal to the grid-scale mean, and this is again a reasonable first guess. The last consists in assuming that the subgrid-scale variance is equally distributed among the different harmonics, a "white" spectrum hypothesis already made to treat convective GWs by *Lott and Guez* [2013], where the variations of the subgrid-scale precipitation equal the grid-averaged precipitation.

From this, and to estimate the launched EP flux, we approximate the buoyancy frequency by $N^2 \approx g\bar{\theta}_{0,z} / \theta_r$. Substituting in (1) gives for each wave number

$$\mathcal{F}_n = \frac{\rho_r}{4} \frac{N}{f} \left(\hat{\zeta}_n \sigma_z\right)^2 e^{-\pi\sqrt{J}}. \tag{3}$$

It is important to keep in mind that we are assuming that the amplitude of each wave is equal to the grid-scale vorticity anomaly $\zeta_r : \hat{\zeta}_n = \zeta_r$. So far, equation (1) has been used for a given vertical level, so we integrate equation (3) vertically to compute the total momentum flux emitted,

$$\vec{F}^{z_l} = G_0 \frac{\Delta z}{4f} \frac{\vec{k}}{\|\vec{k}\|} \int_0^{z_{\text{top}}} \rho_0(z') N(z') \hat{\zeta}^2(z') e^{-\pi\sqrt{J(z')}} \mathrm{d}z', \tag{4}$$

where the n indices have been dropped for conciseness. From (3) to (4), the variable σ_z^2 representing the squared depth of the vorticity anomaly is transformed into the vertical grid spacing $\mathrm{d}z'$ times a tunable depth Δz in (4). Still in (4), z_{top} is the model top altitude, $\rho_0 = \rho_r e^{-z/H}$ is the background density, and G_0 is a tunable parameter of order 1 that controls the amplitude of the EP flux. Here we have simplified the GW momentum flux launched by the large-scale flow at each altitude into a single flux launched from a specific altitude z_l. Although it would be more realistic to launch GWs from each model level, it is more expensive computationally and not necessarily significant since the source term at each level is weighted by density (see equation (4)).

For completeness, we next summarize the procedure to evaluate the GW drag described in *Lott et al.* [2012a]. It is computed as the vertical divergence of the EP flux, and for each wave the EP flux is (i) reduced in the vertical by a small diffusivity μ_d/ρ_0, (ii) limited by that of a saturated wave [*Lindzen*, 1981], and (iii) set to zero immediately above a critical level:

$$\begin{aligned} \vec{F}(z+\delta z) = {} & \frac{\vec{k}}{\|\vec{k}\|} \frac{\Omega}{|\Omega|} \Theta(\Omega(z+\delta z)\Omega(z)) \\ & \min\left\{ |\vec{F}(z)| e^{-2\frac{\mu_d m^3}{\rho_0 \Omega}\delta z}, \rho_r S_c^2 \frac{|\Omega|^3 k_{\min}^2}{N|\vec{k}|^4} \right\}. \end{aligned} \tag{5}$$

In (5) $\Omega = \omega - \vec{k}\cdot\vec{U}$ is the GW intrinsic frequency, the Heaviside function Θ handles critical levels, S_c is a tunable parameter controlling the saturated momentum flux, and $k_{\min}$ is the minimum horizontal wave number allowed. In the case the wave is saturated just above the launching level z_l or if it encounters a critical level between z_l and the next level above, the launching flux becomes the saturated value of the flux or is null. Finally, the GW drag at each model time step is calculated taking into account that the life cycle of the waves (typically $\Delta t \sim 1$ day) is larger than the "physical" time step of the GCM (typically $\delta t < 1$ h). To do so, the forcing produced by the M waves launched at each model time step δt is redistributed over a larger time Δt via an autoregressive relation (see *Lott et al.* [2012a] for details). This way, a few hundred waves act at each model step, which gives an excellent spectral resolution at a cheap computational cost.

The tuning of the FGWD scheme has been done so LMDz has a reasonable zonal mean climatology in the stratosphere and lower mesosphere (see section 4). We launch $M = 8$ waves near the surface (z_l) in the zonal direction every time step, choosing randomly the GWs horizontal wave number within the interval $k_{\min} \le \|\vec{k}\| \le k_{\max}$, with $k_{\max} = 10^{-3}$ m^{-1} and $k_{\min}$ being related to the grid dimensions. The intrinsic phase speed is also randomly chosen from a Gaussian distribution of mean 0 m s^{-1} and standard deviation 40 m s^{-1}. The parameters controlling the saturated flux, the launched flux, and the vertical depth of the PV anomaly are set to $S_c = 0.4$, $G_0 = 3$, and $\Delta z = 1$ km, respectively.

3. GW Stress and Intermittency

We start by showing results from off-line runs using daily data from the European Centre for Medium-Range Weather Forecasts Reanalysis ERA-Interim (ERAI). The main difference with an online setup is that here the time step δt is daily, so $M = 8$ waves are launched every day.

Figure 1a displays the absolute momentum flux launched (i.e., the average of the amplitudes of the individual GW surface stresses) by FGWD (shaded) for a particular day in January 2010. The GW stress is stronger in the midlatitudes, particularly in the Northern Hemisphere, and presents pronounced regional variations with peak values larger than 60 mPa. To illustrate that the GWs are essentially emitted from fronts, we superimpose the 0.012 K km^{-1} isopleth of the horizontal temperature gradient norm $\|\vec{\nabla}_H T\|_{0.012}$ at 600 hPa (black contour). We choose here the 600 hPa level because it is the one taken by *Richter et al.* [2010] on the basis that this closely corresponds to the typical steering level of fronts. The spatial correspondence between the

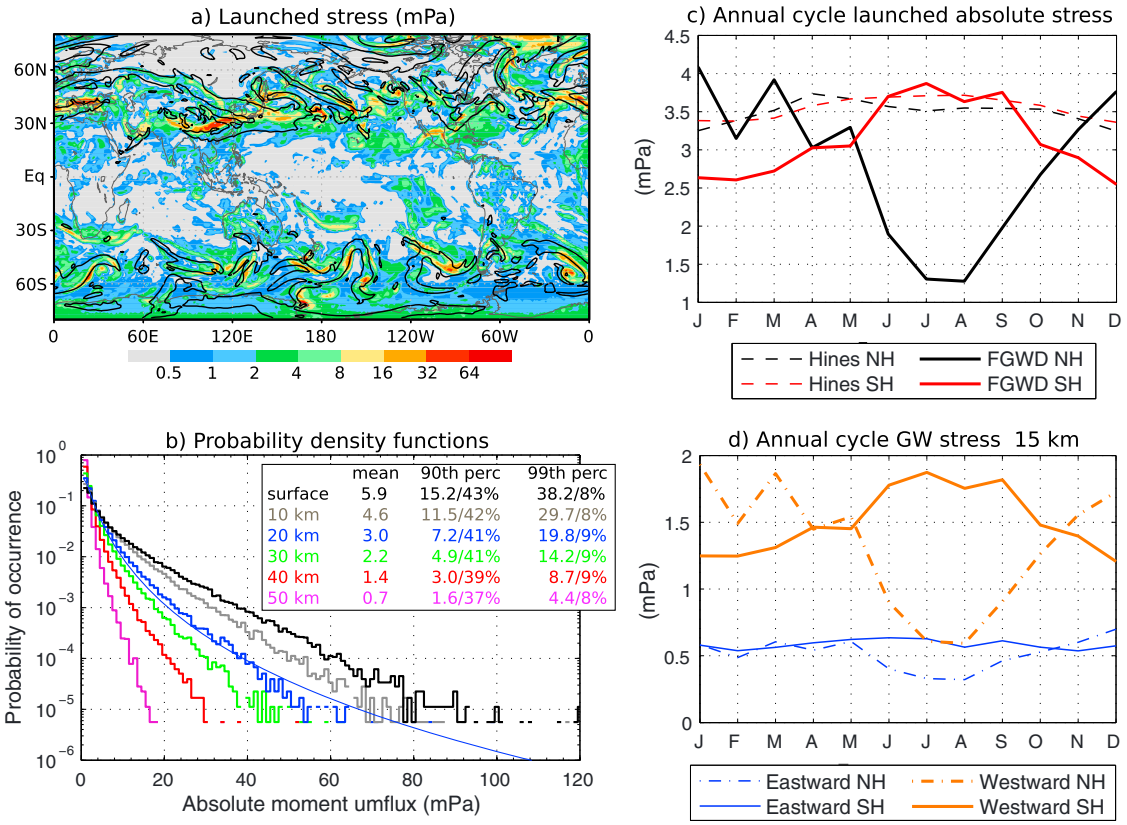

Figure 1. Diagnostics predicted off-line with ERAI and Global Precipitation Climatology Project data. (a) Frontal launched GW stress in mPa (shaded), and the 0.012 K km^{-1} isoline of $\|\vec{\nabla}_H T\|$ at 600 hPa, for the 1 January 2010. (b) PDFs of absolute momentum flux from the source-related nonorographic GW schemes (frontal + convective) for October 2010 over the Southern Ocean (65°S–50°S). The continuous blue line is a lognormal fit of the PDF at 20 km. For each distribution, the (arithmetic) mean, and 90th and 99th percentiles are displayed (in mPa). The percentages of total flux associated with fluxes larger than the percentiles are also indicated. (c) Annual cycle (for the year 2010) of zonal mean surface stress at midlatitudes (Northern Hemisphere (NH): 30°N–60°N and Southern Hemisphere (SH): 60°S–30°S) from FGWD and the *Hines*'s [1997] scheme as indicated, and (d) annual cycle of the eastward and westward components of the frontal GW stress at 15 km height.

GW stress and $\|\vec{\nabla}_H T\|_{0.012}$ is quite satisfactory; practically all the more intense events lay in regions bounded by $\|\vec{\nabla}_H T\|_{0.012}$. However, the GW surface stress is a vertically integrated quantity (see equation (4)), and thus, one should not expect a perfect agreement with fronts detected at a given altitude. In fact, the high stress values at around 180°E–25°S and 105°W–25°N have better agreement with $\|\vec{\nabla}_H T\|$ at 300 hPa, coinciding with locations of two upper level fronts (not shown).

An important factor that needs to be well represented in parameterizations is the GW momentum flux intermittency. Recent observational and modeling studies have detected large instantaneous departures of momentum fluxes from their time averages [e.g., *Hertzog et al.*, 2012; *Wright et al.*, 2013], and this has a crucial impact on the altitudes where the GWs break and force the large-scale flow [*Lott and Guez*, 2013]. One way of evaluating intermittency is to analyze probability density functions (PDFs) of absolute momentum fluxes [e.g., *Hertzog et al.*, 2012], as shown in Figure 1b at different heights over the Southern Ocean (65°S–50°S) for October 2010. These PDFs have been computed considering the GWs from fronts (with FGWD) and convection [see *Lott and Guez*, 2013], which are the two schemes that treat the nonorographic GWs in LMDz (section 4). To compute the PDFs, we sort the momentum fluxes in bins of 1 mPa wide and construct histograms.

Figure 1b shows that values higher than 15.2 mPa at the launching altitude (the 90th percentile) account for 43% of the total flux, whereas the probability of being observed is 10%. Hence, the rather long tails in the PDFs, especially at lower levels in the stratosphere, account for the intermittent nature of the GW field, with rare large events carrying a significant part of the total momentum flux. For completeness, note that the GWs generated by convection have a weaker contribution than those from fronts to the

total momentum fluxes, and thus to these PDFs, at the latitudes considered [*de la Cámara et al.*, 2014]. Figure 1b also shows that the distributions adjust fairly well to a lognormal at 20 km, which qualitatively agrees with observational and modeling studies for nonorographic GWs over the Southern Ocean [*Hertzog et al.*, 2012; *Plougonven et al.*, 2013]. According to *de la Cámara et al.* [2014], this is in good part due to lognormal PDFs in GWs sources, provided that they are related to precipitation and vorticity. In addition, Figure 1b shows that the momentum flux reduction with height mainly affects the tail of the distribution since high-amplitude waves tend to break at lower altitudes in the atmosphere. However, percentages of the total flux represented by the 90th and 99th percentiles do not vary significantly with altitude.

Since the launched GW stress is related to frontal location and intensity, it now presents an annual cycle linked to that of the sources (Figure 1c, solid lines). The GW stress is larger during the extended winter months of both hemispheres and drops down during the summer, especially in the Northern Hemisphere. Still, part of this annual cycle may arise from that of the wind at the launching level, which filters part of the wave spectrum. To evaluate this effect, Figure 1c shows the zonal mean GW absolute stress computed off-line with the *Hines*'s [1997] scheme (dashed lines), in a version still operational in LMDz [*Lott and Guez*, 2013]. The Hines scheme imposes spatially uniform fluxes that are filtered out by the background wind at the launching altitude. It is clear that the annual cycle is much weaker than in FGWD.

The specification in the FGWD scheme of intrinsic (i.e., relative to the background wind) wave phase speeds naturally bias the momentum fluxes launched toward the eastward component, although the effect is small since the waves are emitted near the surface where the wind velocity is small. At 15 km, the westward component clearly dominates the momentum flux of frontal GWs entering the lower stratosphere (Figure 1d). This is in good part due to the intense wave filtering of the eastward component by the tropospheric westerlies between the altitude of emission and 15 km. These results are qualitatively and quantitatively similar to those shown by *Richter et al.* [2010] with a frontogenesis-based parameterization.

4. Online Tests

We use a version of the LMDz GCM with a $3.75° \times 1.875°$ longitude-latitude grid, and 71 levels in the vertical with the top at 1 Pa, and a vertical resolution of around 1 km in the lower stratosphere. For the frontal GW scheme, the online setup is as described in section 2 and we launch $M = 8$ waves at every model step $\delta t = 30$ min. We also use the stochastic GW parameterization linked to convection [*Lott and Guez*, 2013], and the subgrid-scale orography scheme described by *Lott* [1999]. We show results from a control run of 5 years, which will be referred to as LMDz-FC, forced with climatological fields of sea surface temperature, sea ice, soil temperature, and composition over land.

Figures 2a and 2b display the zonal mean zonal drag due to frontal and convective GWs averaged over January in the LMDz-FC. Both frontal and convective GWs exert a negative (positive) acceleration in the winter (summer) stratosphere. The frontal GW drag is well distributed latitudinally. It is larger in the summer than in the winter hemisphere, with the maximum around 55°S, in agreement with the GCM simulation with frontal GWs performed by *Richter et al.* [2010]. The convective drag is weaker than the frontal drag in the midlatitudes and presents a secondary maximum in the summer tropics possibly due to the location of maximum momentum fluxes linked to convection over the summer tropical continents [*Geller et al.*, 2013]. In the equatorial stratosphere the forcing helps generate a QBO (not shown), but the magnitude of the averaged drag is too small to be seen with the contour interval used [see *Lott and Guez*, 2013].

The zonal mean zonal wind profile in January is shown in Figure 2c for LMDz-FC. It is compared with ERAI (Figure 2e) and with the LMDz simulation described by *Lott and Guez* [2013] (Figure 2d), where the two parameterizations that treat nonorographic GWs are the Hines's scheme (not linked to wave sources) and the stochastic GW scheme linked to convection (this run will be referred to as LMDz-HC). The general features, such as the stratospheric jets, look similar in both LMDz runs and ERAI. A major difference between the LMDz runs and ERAI is the strength of the easterly jet in the summer stratosphere, being too strong in LMDz. The latitudinal tilt of the easterly jet is also underestimated in LMDz, although it slightly improves in LMDz-FC. The Northern Hemisphere winter jet in LMDz-FC is wider in latitude and has weaker vertical shear than that in LMDz-HC, and in this sense it is also closer to ERAI.

We have verified that LMDz-FC behaves at least as well as LMDz-HC in other seasons and produces a QBO. To briefly illustrate the impact on the annual cycle, we next analyze the timing of the Southern Hemisphere

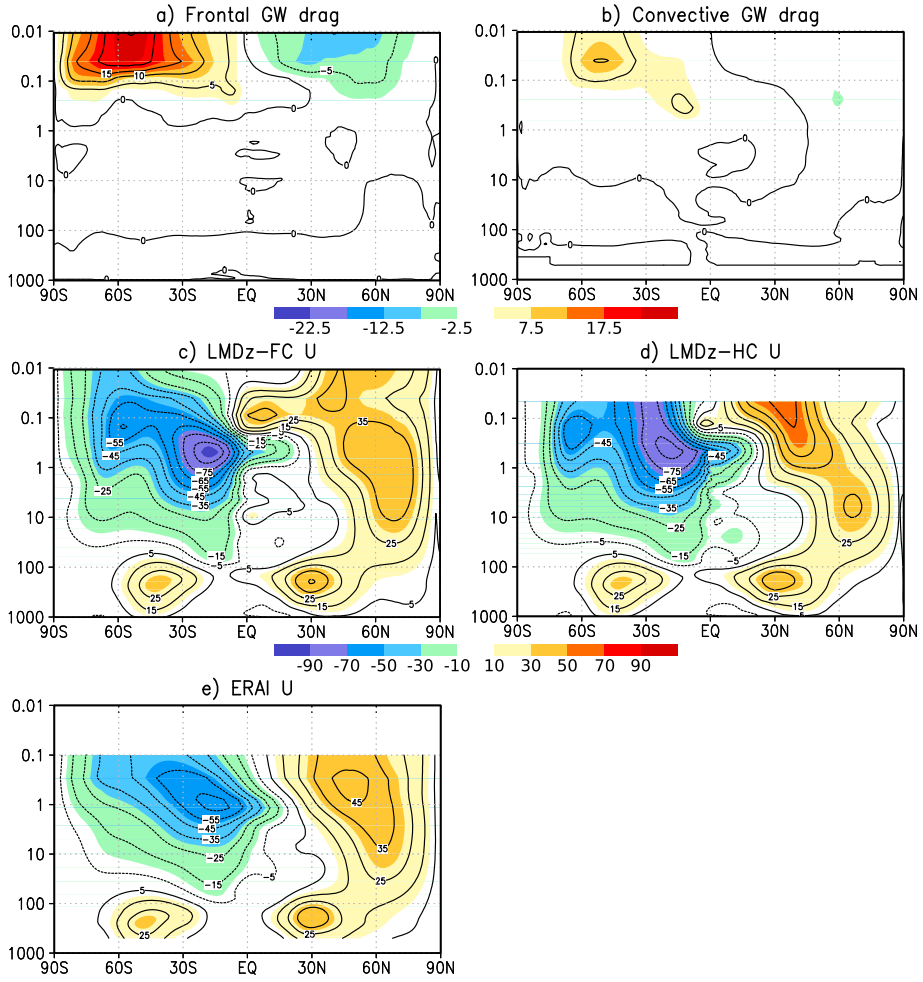

Figure 2. Zonal mean fields averaged for January: GW drag from (a) FGWD and (b) the convective GW scheme (see text), in m s^{-1} d^{-1}. Zonal wind profiles from (c) LMDz-FC, (d) LMDz-HC, and (e) ERAI, in m s^{-1}. For LMDz, 5 year means are used. For ERAI, data from 1979 to 2012 are used.

vortex breakup in the austral spring (i.e., the so-called stratospheric final warming), an important actor of surface climate variability [*Black and McDaniel*, 2007] that is still not well predicted by climate models [e.g., *Eyring et al.*, 2010; *Butchart et al.*, 2011; *Wilcox and Charlton-Perez*, 2013]. This is in part attributed to a deficit in parameterized GW drag around 60°S, but the origin (orographic versus nonorographic GWs) is still controversial [see *McLandress et al.*, 2012; *Alexander and Grimsdell*, 2013; *Hendricks et al.*, 2014]. Figure 3 shows the descent of the zero-wind line at 60°S during the southern spring. LMDz-FC performs just as good as LMDz-HC, eventually being slightly closer to ERAI. This feature deserves further analysis with longer model runs.

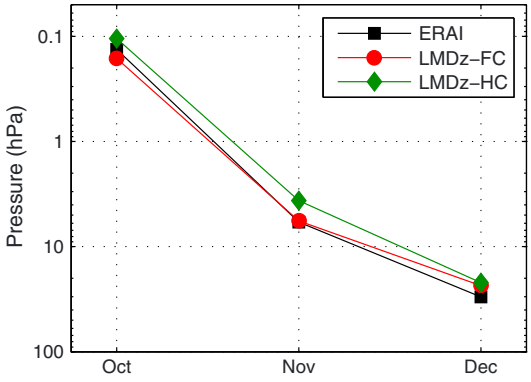

Figure 3. Descent of the zero zonal mean wind line at 60°S calculated from 5 year means of monthly mean data. For ERAI, data from 1979 to 2012 are used.

5. Discussion

Classical geostrophic adjustment, where an initial unbalanced perturbation emits

GWs when it evolves toward the part of the flow that is entirely described by the initial PV anomaly, has long been seen as a potential source of the GWs present in the middle atmosphere. Nevertheless, it is still a challenge to establish the significance of this mechanism for the large-scale circulation: we lack a clear understanding of the forcings that push the flow out of balance, and it is also extremely difficult to diagnose the part of the response that is balanced from that characterized by GWs [*Lott*, 2003]. *Lott et al.* [2010] and *Lott et al.* [2012b] partly solved this problem by evaluating the GW momentum flux emitted *spontaneously* by PV anomalies. Although we know that this only accounts for a fraction of the GW signal (they neglect the classical adjustment mechanism and only consider spontaneous adjustment), the exact formula they derived has the interest of being quantitative and pointing to regions of intense PV anomalies and strong vertical shear. All these ingredients can well be used to predict GWs coming from fronts, which are places characterized by those properties. This permits to bypass all the difficulties inherent to the evaluation of a frontogenesis function and to speculate about the fraction of the GWs that potentially forces this function.

The parameterization was first tested off-line to characterize the annual cycle and the GW intermittency. Probability density functions of absolute momentum fluxes compare well with those observed by superpressure balloons and satellite measurements [*Hertzog et al.*, 2012]. As anticipated by *de la Cámara et al.* [2014], this last result is in good part due to relating explicitly the parameterized GW field to their midlatitude sources. Then it was tested online in the LMDz GCM, and the results obtained are promising. The drag produced compares well with that predicted by state-of-the-art nonorographic schemes, and both the zonal mean winds and the timing of the southern stratospheric final warming are reasonably well simulated by the LMDz GCM with source-oriented GW parameterizations. This is a key first step when introducing important changes in the physics of a climate model, but it is also an important conceptual step: a well-understood theory can be used to produce the right amount of GW drag.

It is difficult to tell if spontaneous adjustment is sufficient to predict all the GWs issued from fronts. When we started testing equation (1) in realistic configurations, we expected to use a large "tuning" factor to obtain the required fluxes (i.e., $G_0 \gg 1$ in equation (4)). This was finally not the case, and our stochastic scheme performs as well as existing parameterizations with arbitrary sources. This is of interest not only to climate modelers but also to theorists and researchers conducting experiments on spontaneous GW emission in balanced flows. Nevertheless, there are large discrepancies between the fluxes measured in situ by the last superpressure balloon campaign in Antarctica (Concordiasi campaign, see *de la Cámara et al.* [2014]) and those deduced from previous balloon campaigns in Antarctica [*Hertzog et al.*, 2012], satellites and models [*Geller et al.*, 2013]. Concordiasi instruments resolve the entire GW spectrum and measure much larger fluxes in the lower stratosphere than the other data sets, and we do not really know today how a GCM could respond to these large fluxes. A possible solution may lie on the reproduction of observed intermittency in parameterizations, where GWs with large momentum fluxes will break and force the circulation at lower altitudes [*Lott and Guez*, 2013; *de la Cámara et al.*, 2014].

In the present paper we have not gone into much detail about the interest of using a stochastic parameterization to represent frontal GWs, we assume that the general interest of stochastic techniques is sufficiently well discussed by *Lott et al.* [2012a] and *Lott and Guez* [2013]. Still, the impact on the large-scale variability of the intermittency introduced by both the sources (convective and frontal) and the stochastic approach remains to be assessed. In addition, introducing GW sources in parameterizations adds more realism to the way GWs are represented in GCMs [*Richter et al.*, 2010]. This is essential because (i) stratospheric processes strongly influence surface climate and middle atmospheric dynamics are partly controlled by GWs, (ii) source-related GW parameterizations introduce a more realistic annual cycle in the GW activity linked to that of the sources, and (iii) the GW sources change in a changing climate, allowing the evaluation of GW effects in future climate conditions [*Palmeiro et al.*, 2014].

Acknowledgments

We thank the Editor Paul D. Williams and two anonymous reviewers for their insightful comments, which helped improve the manuscript. This work was supported by the European Commission's 7th Framework Programme, under the project EMBRACE (grant agreement 282672) and by the French ANR project STRADYVARIUS. ERA-Interim data are provided by the European Centre for Medium-Range Weather Forecasts, from their website at http://apps.ecmwf.int/datasets/. The authors acknowledge the International Space Science Institute in Bern for hosting two one-week workshops about gravity waves observations and parameterization.

The Editor thanks two anonymous reviewers for their assistance in evaluating this paper.

References

Alexander, M. J., and A. W. Grimsdell (2013), Seasonal cycle of orographic gravity wave occurrence above small islands in the Southern Hemisphere: Implications for effects on the general circulation, *J. Geophys. Res. Atmos.*, *118*, 11,589–11,599, doi:10.1002/2013JD020526.

Beres, J. H., M. J. Alexander, and J. R. Holton (2004), A method of specifying the gravity wave spectrum above convection based on latent heating properties and background wind, *J. Atmos. Sci.*, *61*, 324–337.

Black, R. X., and B. A. McDaniel (2007), Interannual variability in the Southern Hemisphere circulation organized by stratospheric final warming events, *J. Atmos. Sci.*, *64*, 2968–2974, doi:10.1175/JAS3979.1.

Borchert, S., U. Achatz, and M. D. Fruman (2014), Gravity waves emission in an atmospheric-like configuration of the differentially heated rotating annulus experiment, *J. Fluid Mech.*, *758*, 287–311, doi:10.1017/jfm.2014.528.

Butchart, N., et al. (2011), Multimodel climate and variability of the stratosphere, *J. Geophys. Res.*, *116*, D05102, doi:10.1029/2010JD014995.

Charron, M., and E. Manzini (2002), Gravity waves from fronts: Parameterization and middle atmosphere response in a general circulation model, *J. Atmos. Sci.*, *59*, 923–941.

de la Cámara, A., F. Lott, and A. Hertzog (2014), Intermittency in a stochastic parameterization of nonorographic gravity waves, *J. Geophys. Res. Atmos.*, *119*, 11,905–11,919, doi:10.1002/2014JD022002.

Eckermann, S. D. (2011), Explicitly stochastic parameterization of nonorographic gravity wave drag, *J. Atmos. Sci*, *68*, 1749–1765, doi:10.1175/2011JAS3684.1.

Eyring, V., T. G. Shepherd, and D. W. Waugh (Eds.) (2010), *Evaluation of Chemistry-Climate Models, Rep. 5, WCRP-132*, WCRP, Geneva, Switzerland.

Geller, M. A., et al. (2013), A comparison between gravity wave momentum fluxes in observations and climate models, *J. Clim.*, *26*, 6383–6405, doi:10.1175/JCLI-D-12-00545.1.

Hendricks, E. A., J. D. Doyle, S. D. Eckermann, Q. Jiang, and P. A. Reinecke (2014), What is the source of the stratospheric gravity wave belt in austral winter?, *J. Atmos. Sci.*, *71*, 1583–1592, doi:10.1175/JAS-D-13-0332.1.

Hertzog, A., G. Boccara, R. A. Vincent, F. Vial, and P. Cocquerez (2008), Estimation of gravity wave momentum flux and phase speeds from quasi-Lagrangian stratospheric balloon flights: Part II. Results from the Vorcore campaign in Antarctica, *J. Atmos. Sci.*, *65*, 3056–3070, doi:10.1175/2008JAS2710.1.

Hertzog, A., M. J. Alexander, and R. Plougonven (2012), On the intermittency of gravity wave momentum flux in the stratosphere, *J. Atmos. Sci.*, *69*, 3433–3448, doi:10.1175/JAS-D-12-09.1.

Hines, C. O. (1997), Doppler-spread parameterization of gravity-wave momentum deposition in the middle atmosphere: Part 2. Broad and quasi monochromatic spectra, and implementation, *J. Atmos. Sol. Terr. Phys.*, *59*, 387–400.

Holton, J. R. (1983), The influence of gravity wave breaking on the general circulation of the middle atmosphere, *J. Atmos. Sci.*, *40*, 2497–2507.

Lindzen, R. S. (1981), Turbulence and stress owing to gravity wave and tidal breakdown, *J. Geophys. Res.*, *86*, 9707–9714, doi:10.1002/jgrd.50705.

Lott, F. (1999), Alleviation of stationary biases in a GCM through a mountain drag parameterization scheme and a simple representation of mountain lift forces, *Mon. Weather Rev.*, *127*, 788–801.

Lott, F. (2003), Large-scale flow response to short gravity waves breaking in a rotating shear flow, *J. Atmos. Sci.*, *60*, 1691–1704.

Lott, F., and L. Guez (2013), A stochastic parameterization of the gravity waves due to convection and its impact on the equatorial stratosphere, *J. Geophys. Res. Atmos.*, *118*, 8897–8909, doi:10.1002/jgrd.50705.

Lott, F., R. Plougonven, and J. Vanneste (2010), Gravity waves generated by sheared potential vorticity anomalies, *J. Atmos. Sci.*, *67*, 157–170, doi:10.1175/2009JAS3134.1.

Lott, F., L. Guez, and P. Maury (2012a), A stochastic parameterization of non-orographic gravity waves: Formalism and impact on the equatorial stratosphere, *Geophys. Res. Lett.*, *39*, L06807, doi:10.1029/2012GL051001.

Lott, F., R. Plougonven, and J. Vanneste (2012b), Gravity waves generated by sheared three-dimensional potential vorticity anomalies, *J. Atmos. Sci.*, *69*, 2134–2151, doi:10.1175/JAS-D-11-0296.1.

McLandress, C., T. G. Shepherd, S. Polavarapu, and S. R. Beagley (2012), Is missing orographic gravity wave drag near 60°S the cause of the stratospheric zonal wind biases in Chemistry-Climate Models?, *J. Atmos. Sci.*, *69*, 802–818, doi:10.1175/JAS-D-11-0159.1.

Palmeiro, F. M., N. Calvo, and R. R. García (2014), Future changes in the Brewer-Dobson circulation under different greenhouse gas concentrations in WACCM4, *J. Atmos. Sci.*, *71*, 2962–2975, doi:10.1175/JAS-D-13-0289.1.

Palmer, T. N., G. J. Shutts, R. Hagedorn, F. J. Doblas-Reyes, T. Jung, and M. Leutbecher (2005), Representing model uncertainty in weather and climate prediction, *Annu. Rev. Earth Planet. Sci.*, *33*, 163–193, doi:10.1146/annurev.earth.33.092203.122552.

Plougonven, R., and F. Zhang (2014), Internal gravity waves from atmospheric fronts and jets, *Rev. Geophys.*, *52*, 33–76, doi:10.1002/2012RG000419.

Plougonven, R., A. Hertzog, and L. Guez (2013), Gravity waves over Antarctica and the Southern Ocean: Consistent momentum fluxes in mesoscale simulations and stratospheric balloon observations, *Q. J. R. Meteorol. Soc.*, *139*(670), 101–118, doi:10.1002/qj.1965.

Richter, J. H., F. Sassi, and R. R. Garcia (2010), Toward a physically based gravity wave source parameterization in a general circulation model, *J. Atmos. Sci.*, *67*, 136–156, doi:10.1175/2009JAS3112.1.

Schirber, S., E. Manzini, and M. J. Alexander (2014), A convection-based gravity wave parameterization in a general circulation model: Implementation and improvements on the QBO, *J. Adv. Model. Earth Syst.*, *6*, 264–279, doi:10.1002/2013MS000286.

Song, I.-S., and H.-Y. Chun (2005), Momentum flux spectrum of convectively forced internal gravity waves and its application to gravity wave drag parameterization: Part I. Theory, *J. Atmos. Sci.*, *62*, 107–124.

Wilcox, L. J., and A. J. Charlton-Perez (2013), Final warming of the Southern Hemisphere polar vortex in high- and low-top CMIP5 models, *J. Geophys. Res. Atmos.*, *118*, 2535–2546, doi:10.1002/jgrd.50254.

Wright, C. J., S. M. Osprey, and J. C. Gille (2013), Global observations of gravity wave intermittency and its impact on the observed momentum flux morphology, *J. Geophys. Res. Atmos.*, *118*, 10,980–10,993, doi:10.1002/jgrd.50869.

Warner, C. D., and M. E. McIntyre (1996), On the propagation and dissipation of gravity wave spectra through a realistic middle atmosphere, *J. Atmos. Sci.*, *53*, 3213–3235.

Williams, P. D., T. W. N. Haine, and P. L. Read (2005), On the generation mechanisms of short-scale unbalanced modes in rotating two-layer flows with vertical shear, *J. Fluid Mech.*, *528*, 1–22, doi:10.1017/S0022112004002873.

Williams, P. D., T. W. N. Haine, and P. L. Read (2008), Inertia-gravity waves emitted from balanced flows: Observations, properties, and consequences, *J. Atmos. Sci.*, *65*, 3543–3556, doi:10.1175/2008JAS2480.1.